OPTICS, LASERS, AND QUANTUM ELECTRONICS

E.YA. GLUSHKO

V.E. Lashkaryov Institute of Semiconductor Physics, Nat. Acad. of Sci. of Ukraine
(41, Prosp. Nauky, Kyiv 03028, Ukraine)

ISLAND-KIND 2D PHOTONIC CRYSTAL RESONATOR

A binary island-kind photonic crystal resonator is investigated analytically and numerically in the framework of the standing wave expansion method. The photonic bandgap structure for a finite SiO_2/SiO_2 resonator with rectangular elementary cell of micron sizes is first calculated. The classification concept of resonator's modes is proposed. The field distribution inside the resonator is calculated, and some ways to use the island resonators in optical devices are discussed.

K e y w o r d s: photonic bandgap materials, photonic resonators, trapped modes.

1. Introduction

At the present time, photonic crystals (PhCr) have been widely investigated as perspective objects of optical technologies in computing, signal processing, telecommunication, sensing *etc.* [1, 2]. The structure of optical spectra of photonic crystals is important for applications in optoelectronic and all-optical devices. In the main, the 2D PhCr is considered as a perfect reflecting medium surrounding an optical waveguide. Therefore, the conditions of omnidirectional gaps in a photonic spectrum are of interest for the determination of the optimal wavelength range of optical devices [3–6].

The further development of this area may be related to a more detailed consideration of the influence of resonator's finite sizes on the modal structure and features of a field modal distribution inside a finite photonic crystal. A number of FDTD investigations devoted to the wave transmission through the infinite 2D PhCr of various symmetries exist (see review [7]). The proposed island 2D resonator is a generalized kind of a 2D photonic crystal, $(N_Z, N_Y \rightarrow \infty)$, and has finite sizes in two directions and perfect ex-

ternal faces (Fig. 1). In [8, 9], the properties of finite resonators were estimated in the framework of perturbation theory. It was found there that a small parameter exists for the problem of the electromagnetic field captured within the total internal reflection (TIR) domain in a finite dielectric structure with the spatially piecewise alternating index of refraction. The condition of existence of a small parameter is based on the demand that the electromagnetic energy inside the resonator be much more than the energy of the mode tails outside the resonator. Therefore, the number of periods in both directions should be more than 10–12. The existence of a small parameter and an appropriate realization of perturbation theory were demonstrated in [8, 9] in the case of weak intrinsic optical contrast of a dielectric photonic structure (see [10]). It was found in [11] that, depending on the geometry, the optical contrast of structures with two types of local states of an electromagnetic field may exist inside a 1D resonator with TIR for several kinds of transmitted and standing waves in a waveguide. It is worth noting that the intrinsic local states arise due to defects of a structure in the bulk of the PhCr, whereas the existence of surface states depends on system's optical contrast. In the proposed 2D island-kind res-
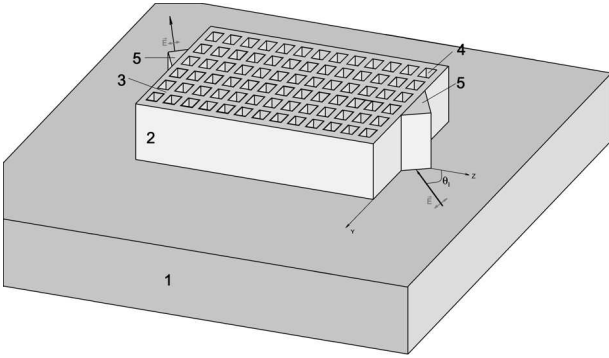
Fig. 1. Sketch of the island-type binary 2D photonic crystal resonator (ICPR). Substrate *1*; covering layer *2*, matrix material *3*, accompanying material (shown air wells) *4*, input-output prisms *5*, θ_1 is the angle of incidence of a *p*-polarized plane wave

onators, the edge local states as a combination of surface states may become possible.

In Fig. 1, a binary island-kind $N_Z \times N_Y$ period photonic crystal resonator (IPCR) grown in the *ZY* plane on a substrate *1* and consisting of matrix material *3* with refractive index n_1 pierced with a regular system of wells/bars *4* having refractive index n_2. In the general case, the IPCR has infinite thickness in the *X* direction. If external covering layer *2* consists of the optically nonlinear material, an opportunity arises to control the beam entrance angle into the resonator due to the phenomenon of shifting the bands, which was discussed in [12]. It was shown there that the Kerr nonlinear coating layer leads to the so-called quasishift effect of bands, causing a strong deviation in the transmission and reflection of the light signal introduced into the structure through the input (Fig. 1). It is also worth noting that the matrix material is topologically connected whereas the ordered bars or wells of a concomitant material, which are embedded into the matrix, are disconnected. This circumstance is important for the method to calculate the field in a finite resonator developed below.

The in-plane standing modes in a resonator can be excited by an external source through special inputs *5* and may be controlled due to their nonlinear properties. The photonic modes differ by field density distributions inside the resonator and by their dependences on the frequency and geometry of incidence that may be used in optical devices to control light energy flows and perform logic operations.

In this work, a binary island-kind photonic crystal resonator is investigated analytically and numeri-

cally in the framework of the standing wave expansion (SWE) method. We have calculated the parametric dependences of the energy of modes for a silicon glass resonator and considered a way to classify the resonator's eigenstates. The field distribution inside the resonator is calculated for different parameters, and some ways to use the switching states in optical devices are discussed.

2. SWE Theory for the Electromagnetic Field in a Finite 2D Photonic Crystal

The Standing Wave Expansion (SWE) approach is based on the representation of a 2D eigenstate of a resonator as the expansion in eigenstates produced by two superposed finite binary 1D photonic crystals crossed in the *Z* and *Y* directions . The eigenvalue problem is analytically solved separately for two probe 1D PhCrs, and the resulting 2D basis is generated as a direct production of separated 1D bases $\{|s\rangle_z\}$ and $\{|g\rangle_y\}$ [8], where $s, g = 1, 2, ..., m$, respectively, and the 2D basis size is m^2. Due to the rectangular form of the resonator, the incident angles of waves in the function $|s(\theta_1)g(\theta_1')\rangle$ united in a 2D basis are correlated: $\theta_1 = \pi/2 - \theta_1'$, where the subscript (1) refers to the optically denser matrix medium, and θ_1 is wave's angle of incidence relative to the *Z*-axis in the matrix material. Suppose that the materials constituting the photonic crystal are optically linear, isotropic, and nonmagnetic, and free charges are absent. Then the equation for the electromagnetic field in a continuous medium with piecewise constant refractive index [1]

$$\frac{1}{\varepsilon(z,y)}\Delta\mathbf{E} + \frac{\omega^2}{c^2}\mathbf{E} = 0 \qquad (1)$$

can be expanded in the 2D basis $|s(\theta_1)g(\theta_1')\rangle$ series. The piecewise constant dielectric function $\varepsilon(z,y)$ is factored out through the Laplace operator. In the considered case of *p*-polarization, a convenient basis of functions $M^{sg}(z,y)$ may be built in several ways: on the components of the magnetic field, on the tangential components of the electric field, and on the normal components of the electric induction. The magnetic-field-based set of eigenfunctions was investigated in [8, 9]. Here, we consider the normal components of the electric induction as the modes

---

[1] Due to the piecewise constant dielectric function, the derivation of the coefficient $\varepsilon(z,y)^{-1}$ gives zero.

$M^{sg}(z,y)$ of the initial basis, where $s = 1, ..., s_{\max}$, $g = 1, ..., g_{\max}$. The physical restrictions demand the mode to be a continuous function of the variables z and y, but the derivatives may have a jump, because the standing waves do not convey energy. Below, we study the rectangular photonic crystal resonator based on a 2D terminated binary structure consisting of the topologically connected matrix material and another one – disconnected material *4* (Fig. 1), which looks like a system of rectangular bars. Therefore, the resonator may be divided into different ij areas by the number of periods N_z, N_y in the Z and Y directions, where $i = 0, 1..., 2N_z + 2$, $j = 0, 1, ..., 2N_y + 2$. The outside areas are described by indices $i = 0, 2N_z + 2$, $j = 0, 2N_y + 2$ and the solution of (1) contains at least one factor exponentially decreasing with distance. Inside the IPCR body, the indices i, j run from 1 to $N_z + 1$ or $N_y + 1$. Then a mode in an intrinsic area ij may be presented as

$$M_{ij}^{sg}(z,y) = A_{zi} \sin\theta_i \, \varepsilon_i \, \cos(k_{is}z + \psi_{is}) \times$$
$$\times A_{yj} \sin\theta_j \, \varepsilon_j \, \cos(k_{jg}y + \psi_{jg}), \qquad (2)$$

where $\varepsilon_{i,j}$ denotes the dielectric function in the matter of the resonator area i or j. The amplitudes A_{zi}, A_{yj} and phases ψ_{is}, ψ_{jg} are analytically obtained here in the framework of the 1D problem for two probe crossed photonic crystals inside intrinsic areas $j, i = 1, ..., 2N + 1$; whereas, for the outside areas where $i = 0$ or $j = 0$, the cosines should be replaced by $\exp(-k_{is}z)$ or $\exp(-k_{jg}y)$, respectively. In [12], the analytic procedure for 1D phases and amplitudes was described in detail. The wavefront orientation with respect to the OZ axes is given by the angle $\theta_i = \theta_1$ or θ_2 for odd or even layers of a probe 1D photonic crystals made of the same materials of appropriate geometry [8]. The angles θ_j presented in the Y-part of the basis function are $\pi/2 - \theta_1$ or $\pi/2 - \theta_2$ for odd or even layers, respectively. Here, index 1 corresponds to the matrix material, and index 2 denotes the ordered bars of another material embedded into the matrix. The indices s, g enumerate the eigenstates of two probe 1D problems solved for the Z degree of freedom for the incident angle θ_1 and for the Y direction at the incident angle θ_1'. We have

$$\mathbf{E}_i = (\sin\theta_i, \cos\theta_i)A_{zi}e^{ik_{iz}z} +$$
$$+ (\sin\theta_i, -\cos\theta_i)B_{zi}e^{-ik_{iz}z},$$

$$\mathbf{E}_j = (\sin\theta_j', \cos\theta_j')A_{yj}e^{ik_{jy}y} +$$
$$+ (\sin\theta_j', -\cos\theta_j')B_{yj}e^{-ik_{jy}y}. \qquad (3)$$

The amplitudes A, B ($A^* = B$ in the considered case) are found in the framework of both probe problems from the system of boundary conditions taken at the $2N_{z(y)} + 1$ alternating boundaries [8–12]. Further, the boundary conditions of continuity for the normal component of the electric induction (mode) at both surfaces of each layer of the probe 1D PhCr lead to the system of equations for the unknown amplitudes. In the matrix representation, we have the system of equations

$$\begin{cases} \widehat{R}_l \begin{pmatrix} A_l \\ B_l \end{pmatrix} = \widehat{L}_1 \begin{pmatrix} A_1 \\ B_1 \end{pmatrix} = \\ = \widehat{R}_1^{-1} \, \widehat{L}_2 \begin{pmatrix} A_2 \\ B_2 \end{pmatrix} = \\ = \widehat{R}_2^{-1} \, \widehat{L}_3 \begin{pmatrix} A_3 \\ B_3 \end{pmatrix} = ... \\ = \widehat{R}_{2N}^{-1} \, \widehat{L}_{2N+1} \begin{pmatrix} A_{2N+1} \\ B_{2N+1} \end{pmatrix} = \\ = A_r \widehat{R}_{2N+1}^{-1} \, \widehat{L}_r \begin{pmatrix} \cos\theta_r \\ \varepsilon_r \sin\theta_r \end{pmatrix}, \end{cases} \qquad (4)$$

where $\widehat{L}$, $\widehat{R}$ are the binary matrices of boundary conditions of the probe problem for a layered photonic crystal, indices l ($i, j = 0$) and r ($i, j = 2N_{z(y)} + 2$) describe the external medium, and the topology demands $\varepsilon_l = \varepsilon_r$. The set of 1D functions $\{|s\rangle_z\}$ and $\{|g\rangle_y\}$ should possess the properties of a basis: completeness, orthogonality, and right positions and number of nodal points. Nevertheless, we observed the affinity of the calculated basis expressed in a weak (5%) nonorthogonality between states of the same parity. We suppose that the 1D basis affinity is caused by jumps of the dielectric function at the layer boundaries. Further, using the Gram–Schmidt procedure of orthogonalization separately for the odd and even subgroups of states, the basis is transformed to the needed orthogonal form.

The expansion of the mode σ in a series gives

$$M_\sigma(z,y) = \sum_{s,g} h_{sg}^\sigma |s,g\rangle. \qquad (5)$$

Then Eq. (1) generates the system of equations for the expansion amplitudes h_{sg}:

$$\begin{cases} \sum_{s,g} \left[\left\langle q \left| \dfrac{k_{sg}^2}{\varepsilon(z,y)} \right| s,g \right\rangle - \dfrac{\Omega^2}{c^2}\delta_{q,sg} \right] h_{sg} = 0, \\ q = 1, ..., N_m, \end{cases} \qquad (6)$$

where q numbers states of the probe 2D basis $|q\rangle = |s', g'\rangle$, $N_m = s_{\max} g_{\max}$, matrix element $\langle q | k_{sg}^2 / \varepsilon(z, y) | s, g\rangle$ means the integral over the resonator and surrounding medium, wave vector k_{sg} is also piecewise continuous constant. It should be noted that the matrix elements have the analytic form in our approach, because the modes M presented in formula (2) are described by the amplitudes $A_{zi}(s)$, $A_{yj}(g)$ and phases ψ_{is}, ψ_{jg} found in two 1D problems for crossed layered structures [8]. These two problems play the role of a 2D basis generator. The full solution of the IPCR system is given by a multitude of eigenvalues Ω_σ^2 and corresponding standing waves, resonator modes:

$$\left\{ \Omega_\sigma^2, \begin{pmatrix} h_1^\sigma \\ ... \\ h_{N_m}^\sigma \end{pmatrix} \right\}, \tag{7}$$

where σ enumerates standing waves inside the total internal reflection area of the resonator, h_m^σ are coefficients of the 2D state σ expansion in the initial basis $|s, g\rangle$ series.

The developed approach differs from the calculation methods for infinite structures like the Plane Wave Expansion Method (PWEM) due to the essential nonperiodicity of the integrals $\langle q | k_{sg}^2 / \varepsilon(z, y) | s, g\rangle$ in (6) that leads to additional $4(N_z + 1)(N_y + 1)$ separate integrals for the total number of ij areas. As a result, the modes σ described by expansion coefficients h_{sg}^σ are far from the periodicity along the IPCR body. As an advantage of this method, one can note that the number of states $|s, g\rangle$ taken to form the 2D basis may be essentially less than in the case of PWEM due to their initial nearness to the needed solutions. In addition, the multitude of states $|s, g\rangle$ can be formed in accordance with the energy interval under consideration.

3. Mode Energy Angular Diagram for an Island Resonator

The island-kind photonic resonator being principally a finite-size object serving to concentrate the electromagnetic energy inside should be described by a basis set of 2D eigenfunctions, which have finite amplitudes in the resonator's volume and decrease to zero outside the IPCR. The electromagnetic flow at the resonance frequency passes into the IPCR through the input and goes out through the output prism (Fig. 1). The gain may be reached due to an appropriate ratio of the input-output sections. One more circumstance is that the IPCR is a convenient system to operate the separate modes due to a distinctive difference in their energies and wave vectors.

We have calculated the 6×7-period (SiO$_2$/SiO$_2$) 2D IPCR consisting of rectangular glass wells with sides $b_z = 1.0$ μm, $b_y = 2.0$ μm and $\varepsilon_2 = 2.25$ periodically distributed in the optically denser glass matrix with the dielectric function $\varepsilon_1 = 3.24$ so that the period is $d_z = a_z + b_z = 2.5$ μm along the Z axis and is $d_y = a_y + b_y = 3.0$ μm along the Y axis. The total sizes of the IPCR are 16×22 microns including the covering layer.

The multitude of modes having the given number of nodal lines forms a branch in the TIR domain (Θ_{TIR}, $\pi/2 - \Theta_{\mathrm{TIR}}$). In Fig. 2, 10 lowest mode branches were calculated for 30 angles θ_1 in interval $0.589 < \theta_1 < 0.982$ (14 mode points at $\theta_1 = \pi/4$). The basis contained 100 eigenfunctions, $s_{\max} = g_{\max} = 10$. The branches $1, 2, ..., 10$ are highlighted by colour. The inclined arrows show the angles of strengthened Bragg diffraction along the symmetry directions: 0.629, 0.657, and 0.695 radians and three symmetrically reflected points with respect to the $\Gamma M'$ direction ($\theta_1 = 0.785$). The calculated lowest energy is $\Omega_{\min} \approx 0.006$ eV (branch 1), the maximal energy 0.372 eV is reached by the mode of branch 9 at $\theta_1 \approx 0.973$, whereas, in interval $(0.922, 0.966)$, both branches 9 and 10 exceed the interval of calculation 0.4 eV. The calculations show that if N_z and N_y increase, then all branches shift down, and the density of branches becomes larger. Therefore, the states existing in an infinite PhCr may be forbidden in a finite resonator.

In some sense, the considered IPCR represents a generalization of a partial case of infinite PhCr, where N_z, N_y should tend to infinity. The local density of modal points along the energy axis increases with N_z and N_y, and, simultaneously, the all modal branches go down. Let us take into account that the number of eigenstates forming the band varies from 0 to N (number of periods in this direction) for the first band, from N to $2N$ for the second one, and so on. Therefore, to transit from the representation of modal branches to the conventional description of the bandgap structure, we should select, step-by-step, N points

$$N = Int \left(\sqrt{N_z^2 \cos^2 \theta_1 + N_y^2 \sin^2 \theta_1} \right) \tag{8}$$
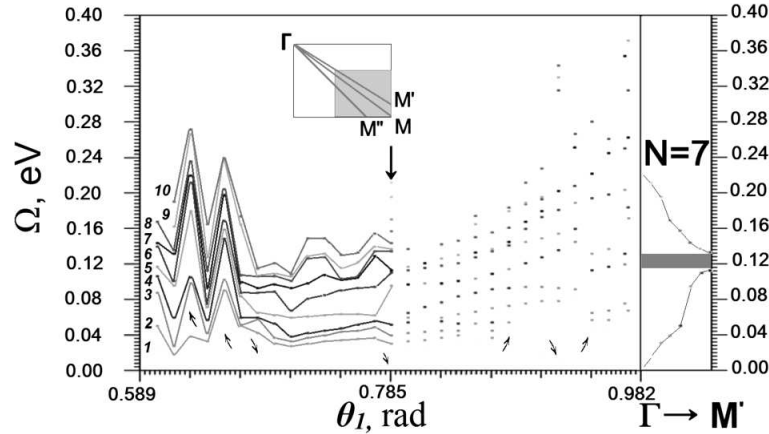
Fig. 2. Mode energy angular diagram of the 6×7-period (SiO$_2$/SiO$_2$) 2D IPCR. *Inset*: rectangular reciprocal lattice cell, symmetry directions: M' corresponds to $\theta_1 = \pi/4$, M is the resonator diagonal, M'' is the elementary cell symmetry direction. *Mode energy diagram*. θ_1 is the plane wave incidence angle in the silicon glass matrix material within the TIR domain $0.589 < < \theta_1 < 0.982$; 1, 2, ..., 10, conventional lines (branches) uniting modal points at different θ_1 by the increased number of nodal lines; $a_y = 1.5$ μm, $a_z = 1.0$ μm, well sizes $b_z = 1.0$ μm, $b_y = 2.0$ μm (bar material *4*, Fig. 1); dielectric functions $\varepsilon_1 = 3.24$ (matrix); $\varepsilon_2 = 2.25$ (bar material *4*); inclined arrows show the angles of strengthened Bragg diffraction; vertical arrow indicates the direction $\Gamma M'$. *Right panel*: generalized bandgap diagram for $\Gamma M'$ direction ($N = 7$), first band, seven points, second band, seven points; gap is between 0.116 and 0.132 eV

corresponding to the chosen angle θ_1. For the $\Gamma M'$ direction ($\theta_1 = \pi/4$), the lowest p-polarized band of the generalized bandgap diagram is shown at the right side of Fig. 2. As far as the number of states in this direction $N = 7$, the first band consists of seven points projected from the $\Gamma M'$ column of mode points (vertical arrow) to right in the order of the mode energy and wavevector growth. In conventional case of an infinite photonic crystal where the number of periods along the chosen direction $\Gamma M'$ goes to infinity, the number of points forming the curve also goes to infinity. The second band contains the next 7 modes numbered from 8 to 14 with energy growth. A partial gap arises between 0.116 and 0.132 eV. In the case of an infinite resonator, the modes become allocated along the band line everywhere densely, though the density of points is expressed by the same formula "crystal size/2π". Here, we consider p-polarized modes of the resonator. The linearly independent set of s-polarized modes forms the own structure of branches, and an additional band line arises in the $\Gamma M'$ direction for each band.

If the resonator has the shape of a square, and if the elementary cells are also squares, the calculated branches become allocated symmetrically as to the bisector $\theta_1 = \pi/4$. In addition, due to the symmetry, the modal branches are doubly degener-

ate. A decrease in the symmetry leads to the splitting of branches, like we can see for the considered IPCR. The SWE approach gives a smooth transformation of the considered IPCR (Fig. 1) to a structure with extremely increased d_y, when the system becomes indistinguishable from a layered structure. Since the angular discreetness of the spectrum arises due to the finite size of the resonator, we have got N angle-dependent mode branches inside every band of states [8–12].

4. Mode Energy Distribution Throughout the Island Resonator

The classification of the modes trapped inside the resonator is ruled by the Courant nodal line theorem [13, 14] claiming that, for a system defined in the space R^m, the nodal set of eigenfunctions (modes) of Eq. (1) is locally composed of hypersurfaces of dimensions $m - 1$. In particular, we have, for $m = 2$, a set of nodal lines, which are either closed or having their ends at the definitional domain. Due to the principally unlimited definitional domain of the problem under consideration, the nodal lines must be also nonrestricted. Several topological features should be noted for the modes of a 2D island-kind resonator:
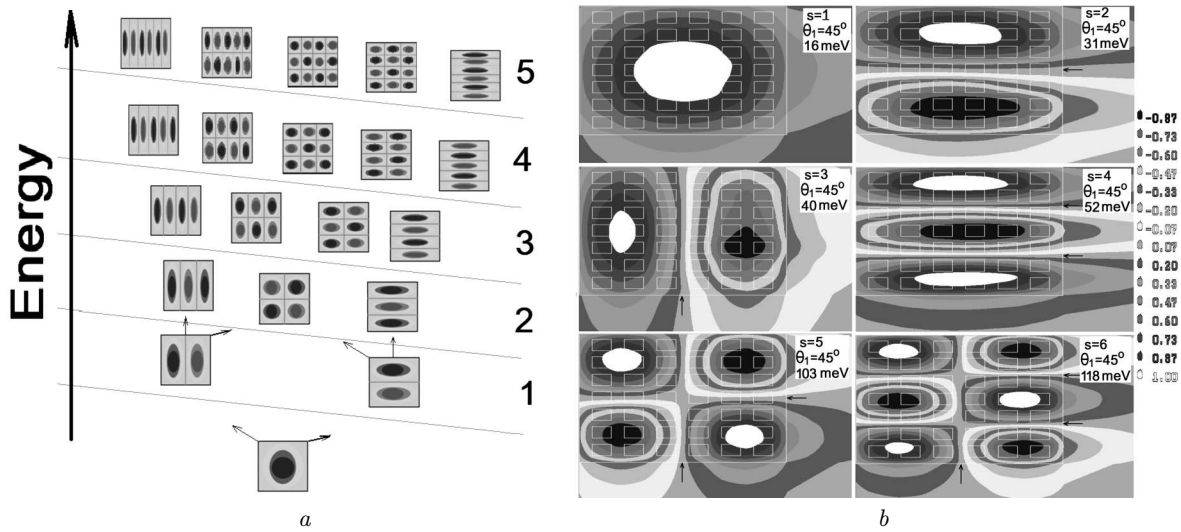
Fig. 3. Classification of eigenstates in an island-kind 2D photonic crystal resonator, lowest 20 modes. Two systems of nodal lines oriented along the Z and Y axes; it is taken that the Y direction has lower energies at the same number of nodal lines, 1, 2, ..., 5 shells of states (*a*); calculated field amplitude distribution for 6 lowest p-polarized modes $s = 1, ..., 6$ with energies of 16, 31, 40, 52, 103, and 118 meV for the 6×7-period (SiO_2/SiO_2), 2D IPCR (parameters are described in Fig. 2), ICPR mask, white lines, black arrows show nodal lines, $\theta_1 = \pi/4$ (*b*)

• The node lines of a mode reflects the symmetry of the system and are divided onto two types: longitudinally (along the Z axis) and transversely oriented.

• The node lines of both types are infinite.

• The energy hierarchy of modes correlates with the number of node lines within a given type.

• If one of two modes has one node line more, it has higher energy, *ceteris paribus.*

The latter statement is the consequence of the easily proved theorem: Between two nodal lines of a mode, one can find a node line of the older mode with higher energy. The Courant nodal line theorem gives a base to test the results of calculations for both the set of mode branches (eigenvalues) and the mode coordinate dependences (eigenfunctions). In Fig. 3, *a*, the classification of the lowest eigenstates in the IPCR is presented. Two factors influence the classification: the number of node lines and a correlation between them. The first circumstance leads to the shell structure of states, when a shell unites modes with the same number of node lines. It is obviously that two types of node lines produce three kinds of modes: with node lines along the Z axis, along Y axis, and containing both transverse and longitudinal node lines. In Fig. 3, *a*, the ground state is represented by a mode without nodal lines, the first shell con-

sists of two modes with 1 node line, second shell contains 3 two-node line states, and so on. In accordance with the Courant theorem, every added node line, even of another type, increases the energy of state. Nevertheless, in a binary structure with rectangular (nonsquare) lattice, the modes containing node lines of one kind may form more or less densely the ladder of energy levels. In particular, if the period $d_y > d_z$, then the modes with transverse node lines have a lowered spectrum. The mixed modes occupy an intermediate position. Therefore, the shells have a tilt that makes the energy hierarchy of states more complicated, like it is shown in Fig. 3, *a*. The above-discussed smooth transformation of the IPCR to a structure with extremely large magnitudes d will manifest itself in an essential reconstruction of the modal structure: the left column remains the same, soft modes containing the transverse node lines become practically indistinguishable from the left column modes with the same number of longitudinal nodal lines and vanish. As a result, the 2D energy angular diagram coincides with the spectral angular diagram of a layered photonic crystal. The mode amplitudes h_m^σ have a sense of a mode expansion coefficients in the $|s, g\rangle$ basis. Following (5) and (6), we calculated the complete eigenvalue problem in-

cluding both energies and eigenfunctions in the basis $s_{\max} = g_{\max} = 10$. In Fig. 3, *b*, the spatial distribution for the lowest 6 modes $\sigma = 1, 2, ..., 6$ at $\theta_1 = 0.785$ is shown. The calculated energies of states Ω_σ are 0.0116, 0.031, 0.040, 0.052, 0.096, and 0.0112 eV. Though the nodal lines allocate in accordance with the Courant theorem (arrows), small deviations from the symmetry in the distribution of modal amplitudes arise due to not too high accuracy of calculations ($\sim$0.01).

The information about the field density distribution in the IPCR may be important in two aspects. First, the pumping of a separate mode inside resonator's TIR domain leads to the accumulation of the energy distributed throughout the IPCR. Therefore, the output beam may be much more intense than the input one. One more circumstance concerns the opportunity to use the matching of distributed active impurities to a chosen mode.

5. Summary

One of the most important challenges of the future technology is the creation of power supercomputers called to solve the global problems of ecology, surviving, economics, scientific investigations, and so on. The awaited expansion from the today existing petaflop computer stations to the exaflop capable machines may be intensified, by using new paradigms both for the element base and design of computers, in particular, like quantum and optical ones. Among the advantages of the use of all-optical principles in logical devices for the optical computing, optical associative memories, and optical interconnections are their higher working frequencies in the signal processing, small energy losses, and practically unlimited possibilities to organize the parallel operating of signals. The all-optical ideology is used to mean the absence of the electronic transforming of signals at any stage of the process, as well as the absence of spin or phonon mechanisms in the signal processing. The reason of all-optical anticipated efficiency in comparison with mixed ways is in an obvious axiom that each signal transformation from one physical form into another form decreases the common speed of passing the signals through a device. The island-kind photonic crystal resonator considered above represents a constructional unit of a logic gate, a medium, where a sum of binary optical signals is transformed into a resulting binary signal. Being mounted on a well-prepared substrate, the IPCR-based logic elements may technologically be united into the integrated circuits of high density to perform the processing of optical signals. The analytic and numerical investigations of a small IPCR made above in the framework of the standing wave expansion method show a well-expressed photonic structure of low-energy eigenstates and field density distribution, which both can be used for the purposes of the signal processing. The 2D basis formation procedure was implemented here with the use of two analytically obtained 1D basis sets for two probe 1D structures and Courant's nodal line theorem in the process of basis generation. Though the rectangular lattice was considered, the proposed SWE method for finite resonators may be adapted to any symmetry of the lattice, as well as for any shape of bars in the matrix.

1. E. Yablonovich. Inhibited spontaneous emission in solid-state physics and electronics. *Phys. Rev. Let.* **58**, 2059 (1987).

2. S. John, D. Joannopoulos, S.G. Johnson, J.N. Winn, R.D. Meade. *Photonic Crystals: Molding the Flow of Light* (2nd ed.) (Princeton Univ. Press., 2008).

3. K. Sakoda. *Optical Properties of Photonic Crystals* (Springer, 2001).

4. N.Y. Winn, S. Fink, Y. Fan, J.D. Joannopoulos. Omnidirectional reflection from a one-dimensional photonic crystal. *Opt. Lett.* **23**, 1573 (1998).

5. M. Deopura, C.K. Ullal, B. Temelkuran, Y. Fink. Dielectric omnidirectional visible reflector. *Opt. Lett.* **26**, 1197 (2001).

6. M. Loncar, T. Doll, J. Vuchkovich, A. Scherer. Design and fabrication of silicon photonic crystal optical waveguides. *J. of Lightwave Technology* **18**, 1402 (2000).

7. C. Jamois, R.B. Wehrspohn, L.C. Andreani, C. Hermann, O. Hess, U. Gösele. Silicon-based two-dimensional photonic crystal waveguides. *Photonics and Nanostruct. – Fundam. and Appl.* **1**, 1 (2003).

8. E.Ya. Glushko, O.E. Glushko, L.A. Karachevtseva. Photonic eigenmodes in a photonic crystal membrane. *ISRN Optics* **2012**, Article ID 373968 (2012).

9. E.Ya. Glushko, O.E. Glushko, L.A. Karachevtseva. Photonic membranes and photonic crystal resonators for all-optical signal processing. *Proc. of SPIE* **7713**, 77131D (2010).

10. E.Ya. Glushko. Influence of oxidation on the photonic spectrum of a ternary comb-like silicon photonic crystal: intrinsic modes, reflection windows and intrinsic contrastivity. *Europ. Phys. J. D* **68**, 264 (2014).

11. E.Ya. Glushko, A.E. Glushko, V.N. Evteev, A.N. Stepa-nyuk. All-optical signal processing based on trapped modes of a photonic crystal resonator. In: *Proc. SPIE* **7354**, 73540L (2009).

12. E.Ya. Glushko. Switching of electromagnetic eigenmodes in metastructures. *Proc. SPIE* **6989**, Article 69891G (2008).

13. R. Courant, D. Hilbert. *Methods of Mathematical Physics* (Interscience, 1953), vol. 1.

14. G.M.L. Gladwell, H. Zhu. Courant's nodal line theorem and its discrete counterparts. *Q. J. Mech. Appl. Math. (Oxford)* **55**, 1 (2002).

Є.Я. Глушко

2D ФОТОННО-КРИСТАЛІЧНИЙ
РЕЗОНАТОР ОСТРІВКОВОГО ТИПУ

Р е з ю м е

Аналітично та чисельно досліджено фотонно-кристалічний резонатор острівкового типу зі застосуванням метода розкладання за стоячими хвилями. Вперше проведено розрахунки фотонної зони кінцевого SiO_2/SiO_2 резонатора цього типу з прямокутною елементарною коміркою мікронних розмірів. Запропоновано концепцію класифікації резонаторних мод. Розраховано розподіл поля для типових мод всередині резонатора та обговорено шляхи використання острівкових резонаторів в оптичних приладах.